Astronomy & Astrophysics manuscript no. SLF_SMC_TASC
June 28, 2024

Photometric detection of internal gravity waves in upper main-sequence stars

IV. Comparable SLF variability in SMC, LMC and Galactic massive stars

Dominic M. Bowman[1,2], Pieterjan Van Daele[2], Mathias Michielsen[2], and Timothy Van Reeth[2]

[1] School of Mathematics, Statistics and Physics, Newcastle University, Newcastle upon Tyne, NE1 7RU, UK
e-mail: dominic.bowman@newcastle.ac.uk
[2] Institute of Astronomy, KU Leuven, Celestijnenlaan 200D, B-3001 Leuven, Belgium

Received XXXX; accepted YYYY

ABSTRACT

Context. Massive main-sequence stars have convective cores and radiative envelopes, but can also have sub-surface convection zones caused by partial ionisation zones. However, the convective properties of such regions strongly depend on opacity and therefore a star's metallicity. Non-rotating 1D evolution models of main-sequence stars between $7 \leq M \leq 40$ $M_{\odot}$ and metallicity of the Small Magellanic Cloud (SMC) galaxy suggest perhaps only marginal sub-surface convection zones when using the Rayleigh number as a criterion for convection owing to their substantially lower metallicity compared to Galactic massive stars.
Aims. We aim to test if massive stars of different metallicities both inside and outside of asteroseismically calibrated stability windows for sub-surface convection exhibit similar or different properties in their observed stochastic low-frequency (SLF) variability. Thus we aim to constrain the metallicity dependence of the physical mechanism responsible for SLF variability commonly found in light curves of massive stars.
Methods. We extract customised light curves from the ongoing NASA Transiting Exoplanet Survey Satellite (TESS) mission for a sample of massive stars using an effective point spread function (ePSF) method, and compare their morphologies in terms of characteristic frequency, $\nu_{\rm char}$, and amplitude using a Gaussian process (GP) regression methodology.
Results. We demonstrate that the properties of SLF variability observed in time-series photometry of massive stars are generally consistent across the metallicity range from the Milky Way down to the SMC galaxy, for stars both inside and outside of the sub-surface stability windows based on the Rayleigh number as a criterion for convection.
Conclusions. We conclude that non-rotating 1D stellar structure models of sub-surface convection cannot alone be used to explain the mechanism giving rise to SLF variability in light curves of massive stars. Additionally, the similar properties of SLF variability across a large range in metallicity suggests that sub-surface convection zones may be more favourable for evolved stars and core-excited internal gravity waves (IGWs) are more favourable for younger stars that lack substantial sub-surface convection zones, especially at low-metallicity. Given the ubiquitous but diverse morphologies of SLF variability in light curves of massive stars across a wide range in metallicity, multiple physical mechanisms are likely responsible which transition in dominance during the main sequence.

Key words. stars: early-type – stars: fundamental parameters – stars: massive – stars: rotation – stars: oscillations

1. Introduction

Our ability to ascertain precise and accurate constraints on the physical processes within massive stars, such as chemical mixing and angular momentum transport, has been revolutionised by studying stellar variability and applying forward asteroseismic modelling — see Bowman (2020) for a review. In the traditional approach, coherent self-excited pulsation modes allow one to perform linear asteroseismology by quantitatively comparing observed pulsation mode frequencies to their theoretical counterparts calculated from a grid of stellar structure models (Aerts et al. 2010; Aerts 2021). The coherent pulsations in massive stars are generally grouped into pressure (p) and gravity (g) modes based on their respective restoring forces, which probe the envelope and deep interior of a massive main-sequence star, respectively. So-called coherent pulsation modes are excited by a periodic heat-engine mechanism operating within the iron-nickel opacity bump at 200 000 K (Dziembowski & Pamyatnykh 1993; Dziembowski et al. 1993; Miglio et al. 2007; Szewczuk & Daszyńska-Daszkiewicz 2017). Important constraints from forward asteroseismic modelling of coherent pulsations include their interior mixing and rotation profiles, magnetic field strength and geometry, and the efficiency of angular momentum transport (Aerts et al. 2003; Dupret et al. 2004; Pamyatnykh et al. 2004; Dziembowski & Pamyatnykh 2008; Briquet et al. 2012; Salmon et al. 2022; Lecoanet et al. 2022; Burssens et al. 2023; Vanlaer et al. 2024).

The necessary data for asteroseismic analyses of massive stars are long-duration time series, either photometric or spectroscopic, spanning at least a few months but ideally several years (Bowman 2023). Given that high-cadence spectroscopic time series are quite expensive when assembled with ground-based telescopes (see e.g. Aerts et al. 2003), asteroseismology using space-mission light curves has largely driven the field during the last two decades. Space missions with an asteroseismic component include CoRoT (Auvergne et al. 2009), BRITE (Weiss et al. 2014, 2021), Kepler/K2 (Borucki et al. 2010; Koch et al. 2010; Howell et al. 2014) and the Transiting Exoplanet Survey Satellite (TESS; Ricker et al. 2015), which together have revealed a

diversity of variability mechanisms at work in massive stars (see e.g. Degroote et al. 2009; Bowman et al. 2019b; Burssens et al. 2020; Zwintz et al. 2024).

Recently a new form of asteroseismic signal called stochastic low-frequency (SLF) variability has been discovered in many massive stars (Bowman et al. 2019a,b), and shown to directly probe a massive star's mass and age (Bowman et al. 2020; Bowman & Dorn-Wallenstein 2022). This SLF variability is seemingly ubiquitous in Galactic massive stars with light curve data of sufficiently high photometric precision. After an initial detection in three O stars observed by CoRoT (Blomme et al. 2011), the first large-scale analysis of SLF variability among massive stars revealed a common morphology for dwarf stars with spectral types earlier than B9 (Bowman et al. 2019a). The sample was expanded to include hundreds of massive stars across the sky using photometry from the K2 mission in addition to dozens of blue supergiants in the Large Magellanic Cloud (LMC) galaxy for the first time (Bowman et al. 2019b). Later, combining TESS mission light curves and high-resolution spectroscopy, it was shown that a strong correlation exists between the properties of SLF variability and the location of stars in the Hertzsprung–Russell (HR) diagram (Bowman et al. 2020). Recently, a novel method using Gaussian process (GP) regression confirmed this correlation, and revealed a transition from stochastic to quasi-periodic variability exists for massive Galactic stars as they evolve during the main sequence (Bowman & Dorn-Wallenstein 2022). In the absence of coherent heat-engine pulsation modes for stars with light curves dominated by SLF variability, it is not possible to apply standard forward asteroseismic modelling methods, thus motivating the advent of gravity wave asteroseismology (Bowman 2023).

Various theoretical and multi-dimensional hydrodynamical model predictions for explaining SLF variability in massive stars exist within the literature, which are not mutually exclusive. Plausible mechanisms put forward include internal gravity waves (IGWs) excited stochastically at the boundary of convective cores (Rogers et al. 2013; Rogers 2015; Edelmann et al. 2019; Horst et al. 2020; Varghese et al. 2023; Ratnasingam et al. 2019, 2020, 2023; Vanon et al. 2023; Herwig et al. 2023; Thompson et al. 2024), waves and/or turbulence caused by sub-surface convection zones (Cantiello et al. 2009, 2021; Schultz et al. 2022), and inhomogeneities in the winds of massive stars (Krtička & Feldmeier 2018; Krtička & Feldmeier 2021). However, the latter of these mechanisms is expected to play a negligible role for late-O and early-B main-sequence stars because of their optically thin and weak winds, especially at low metallicity. The explanation of SLF variability is hotly debated in the literature. Some hydrodynamical simulations suggest that IGWs excited by core convection reach the surface with smaller amplitudes than the typical observed amplitudes for SLF variability, thus postulate that SLF variability arises from another convective region (Lecoanet et al. 2019, 2021; Le Saux et al. 2023; Anders et al. 2023). However, owing to the numerical challenges, hydrodynamical studies have generally not yet been performed using 3D spherical geometry with comparable rotations rates to observed stars, and that include the full spectrum of spherical harmonic geometries expected for IGWs. This makes a quantitative comparison of numerical simulations to observations quite difficult.

Recently, Jermyn et al. (2022) demonstrated using non-rotating 1D stellar structure models that late-O and early-B main sequence stars at low metallicity may not have significant sub-surface convection zones when the Rayleigh number is considered as a necessary criterion for convection. This may call into question if the near-surface layers of massive stars at low metallicity can excite IGWs. Regardless, IGWs generated by turbulent core convection are not mutually exclusive with IGWs generated by sub-surface convection zones. In fact, observations suggest a possible transition between IGWs excited by core convection being dominant at the zero-age main sequence (ZAMS) to IGWs excited by sub-surface convection being dominant at the terminal-age main sequence (TAMS) in the Hertzsprung–Russell (HR) diagram for Galactic massive stars (Bowman & Dorn-Wallenstein 2022). Yet this transition remains unexplored outside of Galactic massive stars.

In this work, paper IV of the current series, we use new TESS observations and advanced light curve extraction techniques to focus in particular on massive stars in the Small Magellanic Cloud (SMC) galaxy and compare them to stars in the LMC and the Milky Way. Our specific goal is to test if a common morphology exists for SLF variability across a wide range in metallicity, keeping in mind the possible absence of sub-surface convection zones in low-metallicity massive stars (Jermyn et al. 2022). In Section 2 we describe the calculation of 1D stellar structure and evolution models to define sub-surface convection stability windows, and in Section 3 we describe our target star selection criteria and TESS light curve extraction methodology. In Section 4, we present and discuss our analysis of the light curves and SLF variability, and we conclude in Section 5.

2. Sub-surface convection stability windows

2.1. Rayleigh number for convection

Recently, Jermyn et al. (2022) investigated the properties of sub-surface convection zones using non-rotating structure models with the 1D stellar evolution code MESA (Paxton et al. 2011, 2013, 2015, 2018, 2019; Jermyn et al. 2023). They specifically looked at whether the envelopes of massive stars satisfy the Rayleigh number as a criterion for convection. The Rayleigh number, Ra, for the onset of convection is defined as:

$$\mathrm{Ra} \equiv \frac{g\left(\nabla_{\mathrm{rad}} - \nabla_{\mathrm{ad}}\right)\delta r^3}{\nu\alpha}\left(\frac{\delta r}{h}\right)\left(\frac{4-3\beta}{\beta}\right) \tag{1}$$

where ∇_{rad} is the radiative temperature gradient, ∇_{ad} is the adiabatic temperature gradient, g is the gravitational acceleration, ν is the kinematic viscosity, α is the thermal diffusivity, h is the pressure scale height, and β is the radiation parameter (cf. Jermyn et al. 2022 and references therein). This Rayleigh number indicates the importance of buoyancy when compared to diffusive processes, such that when $\mathrm{Ra} < \mathrm{Ra}_{\mathrm{crit}}$ buoyancy is insufficient to overcome diffusive processes and convection cannot occur.

Jermyn et al. (2022) used the Rayleigh number to test whether sub-surface convection zones, associated with partial ionisation zones of metals (e.g. iron, nickel), helium and hydrogen, are present for non-rotating 1D models of stars spanning $7 \leq M \leq 40$ $\mathrm{M}_{\odot}$ and ranging from the onset of core-hydrogen burning (i.e. ZAMS) until core-hydrogen exhaustion (i.e. TAMS). Using Eqn. (1) as a condition for convective instability, Jermyn et al. (2022) demonstrated that massive stars with Galactic metallicity always have a sub-surface convection zone within their envelopes during the main sequence. However, for lower metallicities, such as stars in the SMC and LMC galaxies, there seems to exist a parameter space in the Hertzsprung–Russell (HR) diagram for which only the convective core satisfies the Rayleigh number for convection, such that there are no sub-surface convection zones. Jermyn et al. (2022) defined these parameter spaces as 'stability windows' in the HR diagram

in which the partial ionisation zones of metals, hydrogen and helium are not convection zones. Therefore, given the significant differences in the convective properties of stellar envelopes between metal-rich and metal-poor stars, the properties of SLF variability observed in the light curves of such stars may be different if these zones are acting as the physical mechanism responsible for SLF variability.

2.2. Asteroseismic MESA models

In this work, motivated by the numerical predictions of Jermyn et al. (2022), we expand upon the previous grid of 1D non-rotating MESA model calculations by including convective boundary mixing (CBM) and envelope mixing (i.e. $D_{\rm env}$) calibrated by asteroseismology. This is important because interior mixing has a large impact on the width of the main sequence in the HR diagram and the radius and maximum possible age of a massive star at the TAMS. A growing number of asteroseismic studies have demonstrated the importance of a non-negligible amount of CBM in massive main-sequence stars (Dupret et al. 2004; Pamyatnykh et al. 2004; Dziembowski & Pamyatnykh 2008; Briquet et al. 2011; Burssens et al. 2023). In particular, a non-zero amount of CBM facilitates unprocessed hydrogen from the envelope to be transported into the nuclear-burning core, thus extending the main-sequence lifetime by at least 25% and displacing the TAMS to cooler effective temperatures in the HR diagram (Bowman 2020).

We calculate a finely sampled grid of non-rotating evolutionary tracks using MESA (v15140) for stars with masses $7 \leq M \leq 40$ M$_{\odot}$, a metal mass fraction consistent with the SMC (i.e. $Z = 0.002 \simeq 0.2$ Z$_{\odot}$), and ages that span from the ZAMS to the TAMS. We include a fixed amount of envelope mixing (i.e. $\log(D_{\rm env}) = 3.0$) and a range in CBM using the diffusive exponential mixing prescription (i.e. $0.0 \leq f_{\rm ov} \leq 0.3$) (Michielsen et al. 2021) as inferred from detailed forward asteroseismic modelling of pulsating stars within and proximate to this parameter space (e.g. Pedersen et al. 2021; Burssens et al. 2023). For completeness, we also calculate a second grid of MESA models with the same range of parameters as the SMC except that the metal mass fraction is consistent with stars in the LMC (i.e. $Z = 0.006 \simeq 0.5$ Z$_{\odot}$).

Our sub-surface convection zone stability windows that include the full range of CBM inferred from asteroseismology are shown in Fig. 1. The stability windows cover a larger parameter space in the HR diagram compared to those of Jermyn et al. (2022), because of the non-zero amount of CBM. We show the evolutionary tracks with the minimal and maximal values of CBM as solid and dashed lines, respectively, which displaces the TAMS to cooler temperatures and higher luminosities because of the extended main-sequence lifetime being at least 25% longer in massive stars that include non-zero CBM (see Bowman 2020). As expected, the size of the stability window for SMC metallicity is much larger than for LMC metallicity, as previously demonstrated by Jermyn et al. (2022).

3. TESS light curves of low-metallicity massive stars

TESS is an all-sky time-series photometric survey mission observing individual sectors of the sky for up to 27 d (Ricker et al. 2015). Its primary science case is to identify candidate exoplanet transits orbiting bright Galactic stars. TESS provides its entire field of view spanning four cameras as full-frame images (FFIs)

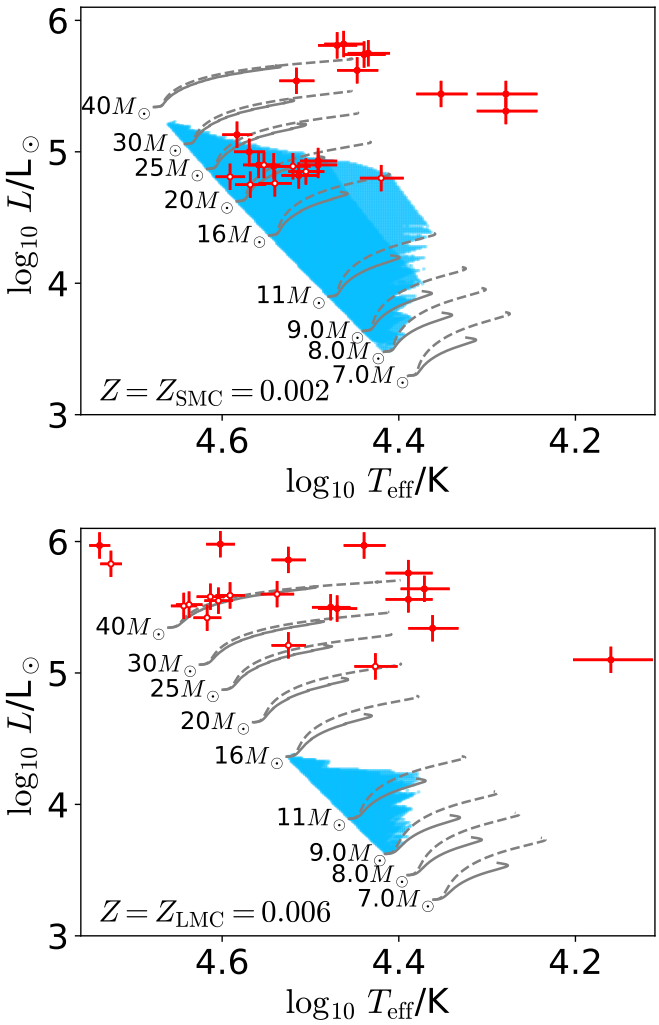

Fig. 1. Hertzsprung–Russell (HR) diagram for SMC stars (i.e. $Z = 0.002$; top panel) and LMC stars (i.e. $Z = 0.006$; bottom panel) with evolutionary tracks of different masses between the ZAMS and the TAMS. The sub-surface convection zone stability windows as defined by the Rayleigh number in Eqn. (1) are shown in blue for evolutionary tracks that encompasses the minimal (solid lines) and maximal (dashed lines) values of CBM as inferred from asteroseismology. The location of the sub-sample of stars with reliable TESS light curves are shown as red points, with filled and open symbols representing stars with confident and marginal detections of SLF variability, respectively.

at a cadence of 200 s as of its second extended mission (Jenkins et al. 2016). Previous FFI cadences were 30 min and 10 min in the nominal mission and first extended mission, respectively. Bias subtraction and flat fielding are performed before delivery of FFIs to the Mikulski Archive of Space Telescopes (MAST[1]).

3.1. SMC and LMC sample selection

As our goal is to investigate the occurrence and properties of SLF variability of massive stars at low metallicity, we require a bona fide sample of massive stars in the SMC and LMC galaxies to place in the HR diagram. Indeed, massive stars, including dwarfs, giants and supergiants of spectral types earlier than about B9 in the LMC have been studied spectroscopically thanks to Very Large Telescope (VLT) programmes with European

[1] https://archive.stsci.edu/missions-and-data/tess

Table 1. SMC massive stars proximate to and within the sub-surface convection zone stability window studied in this work, with spectroscopic parameters from Vink et al. (2023) and Hawcroft et al. (2023) and the characteristic frequency of their SLF variability, $\nu_{\rm char}$, and its 2σ confidence interval from the GP regression methodology of Bowman & Dorn-Wallenstein (2022). An average for the typical reported uncertainties are $\sigma\,(T_{\rm eff})$ = 1500 K and $\sigma\,(\log_{10}\,(L/{\rm L}_\odot))$ = 0.1 dex.

Simbad resolvable name	TIC ID	Gaia DR3	$T_{\rm eff}$ (K)	$\log_{10}\,(L/{\rm L}_\odot)$	$\nu_{\rm char}$ (d^{-1})
Confident detections of SLF variability:					
AzV 16	180617038	4685854571724688768	27200	5.75	$0.33^{+0.08}_{-0.09}$
AzV 18	180617057	4688950933906863488	19000	5.44	$0.35^{+0.17}_{-0.18}$
AzV 83	181043369	4688966125248119808	32800	5.54	$0.88^{+0.13}_{-0.12}$
Cl* NGC 346 MPG 12	181880133	4689016221756858624	31000	4.93	$0.96^{+0.20}_{-0.17}$
Cl* NGC 346 ELS 25	182294030	4690504994818102016	36200	4.90	$0.73^{+0.15}_{-0.13}$
AzV 264	182294249	4690520387983090432	22500	5.44	$0.40^{+0.08}_{-0.09}$
Cl* NGC 346 MPG 682	182300967	4689015465842590464	34800	4.89	$0.73^{+3.54}_{-0.66}$
AzV 372	182729695	4687411518857964032	28000	5.62	$0.48^{+0.09}_{-0.09}$
AzV 429	182910549	4687532533854919680	38300	5.13	$1.03^{+0.24}_{-0.19}$
AzV 479	183306464	4686408759936714752	29000	5.82	$1.05^{+0.18}_{-0.20}$
AzV 472	183306676	4687241472507227520	19000	5.31	$0.49^{+0.08}_{-0.09}$
AzV 488	183492668	4686413437158238208	27500	5.74	$0.56^{+0.10}_{-0.10}$
[M2002] SMC 81469	183979145	4686450580031889536	31000	4.90	$1.99^{+0.39}_{-0.30}$
2dFS 163	267429694	4688838203919272832	32600	4.82	$1.48^{+0.30}_{-0.25}$
AzV 461	402099597	4687470686324401536	37100	5.00	$0.36^{+0.12}_{-0.14}$
AzV 456	402100664	4687251368112248960	29500	5.81	$0.83^{+0.21}_{-0.24}$
Marginal detections of SLF variability:					
AzV 202	181887485	4689019898248677888	26300	4.80	$2.04^{+1.97}_{-0.95}$
Cl* NGC 346 ELS 46	182294016	4690504582501410432	39000	4.81	$2.10^{+9.16}_{-1.74}$
AzV 267	182294155	4690507022042458624	35700	4.90	$1.47^{+6.93}_{-0.63}$
AzV 251	182300503	4685990709381204864	33100	4.89	$2.69^{+10.02}_{-1.11}$
AzV 468	183302393	4687248791131672960	34700	4.76	$7.78^{+16.26}_{-6.98}$
2dFS 3780	183981879	4686448106130736256	32000	4.85	$1.39^{+0.36}_{-0.28}$
2dFS 3954	303910981	4686266721070836608	37000	4.75	$2.95^{+16.79}_{-1.97}$

Southern Observatory (ESO) instruments, such as VLT-Flames (PI: Smart) and its successor the VLT-Flames Tarantula Survey (VFTS; PI: Evans), and more recently the ongoing BLoEM survey for the SMC (PI: Shenar; Shenar et al. 2024). Breakthroughs in studying LMC massive stars include the metallicity dependence of winds and mass loss (Mokiem et al. 2007), empirical rotation rates (Ramírez-Agudelo et al. 2013), surface-nitrogen abundances and their relation to interior mixing (Hunter et al. 2008), and constraints on binary statistics (Sana et al. 2012).

The Hubble Space Telescope (HST) has recently performed an unprecedented number of orbits as part of a Director's Discretionary Time (DDT) project called 'Ultraviolet Legacy Library of Young Stars as Essential Standards' (ULLYSES[2]; Roman-Duval et al. 2020). The ULLYSES project is targeting over 250 massive stars in the SMC and LMC, with the HST data consisting of high-quality COS and STIS UV spectra. To support these data, an ESO large program, X-Shooting ULLYSES (XShootU[3]), has assembled medium-resolution optical spectra with the XShooter spectrograph (Vernet et al. 2011). Spectroscopic parameters, in particular effective temperature and luminosity, are available from the first papers from the XShootU collaboration (Vink et al. 2023; Hawcroft et al. 2023), but are also supplemented by spectroscopic studies by Mokiem et al. (2006) and Bouret et al. (2013).

3.2. TESS light curve extraction

There are two major challenges to overcome for extracting reliable TESS light curves of SMC and LMC stars. We emphasise that the TESS mission was not designed for this purpose, hence specialised software tools are needed and a moderately high failure rate in this work is inevitable. The first major challenge is that distant stars beyond the Milky Way are typically quite faint for the brightness limit of the TESS mission. Second, such stars are usually contaminated since they suffer from high crowding and blending in the relatively large (i.e. 21 arcsec) pixels of TESS's CCDs. These limitations have the potential to severely limit astrophysical inference based on light curves extracted using standard simple aperture photometry (SAP) techniques, which is common for Galactic massive stars (see e.g. Bowman et al. 2022; Burssens et al. 2023).

[2] https://ullyses.stsci.edu
[3] https://massivestars.org/xshootu/

Table 2. LMC massive stars proximate to the sub-surface convection zone stability window studied in this work, with spectroscopic parameters from Vink et al. (2023) and Hawcroft et al. (2023) and the characteristic frequency of their SLF variability, $\nu_{\rm char}$, and its 2σ confidence interval from the GP regression methodology of Bowman & Dorn-Wallenstein (2022). An average for the typical reported uncertainties are $\sigma\,(T_{\rm eff})$ = 1500 K and $\sigma\,(\log_{10}\,(L/{\rm L}_{\odot}))$ = 0.1 dex.

Simbad resolvable name	TIC ID	Gaia DR3	$T_{\rm eff}$ (K)	$\log_{10}\,(L/{\rm L}_{\odot})$	$\nu_{\rm char}$ (d^{-1})
Confident detections of SLF variability:					
Sk −68 41	31105740	4661392533937464448	24500	5.56	$0.42^{+0.05}_{-0.06}$
Sk −68 52	31181554	4661289630893455488	24500	5.76	$0.32^{+0.06}_{-0.07}$
Sk −65 22	55758033	4662240708409788928	33500	5.86	$0.67^{+0.09}_{-0.10}$
VFTS 72	277300368	4657698454092124416	54800	5.97	$1.04^{+0.16}_{-0.16}$
Sk −66 17	277103700	4660278492484698112	29500	5.49	$1.06^{+0.11}_{-0.10}$
Sk −68 135	277300709	4657700790554314752	27500	5.97	$0.24^{+0.09}_{-0.12}$
Sk −71 35	287436747	4651835961162249984	23000	5.34	$0.35^{+0.08}_{-0.10}$
RMC 109	391746326	4660181151347435008	14450	5.10	$0.27^{+0.08}_{-0.10}$
Sk −71 41	391887962	4651834994760055040	30000	5.50	$0.77^{+0.09}_{-0.09}$
Sk −68 140	404768212	4657688313632701568	23500	5.64	$0.48^{+0.09}_{-0.10}$
Sk −67 166	425083410	4660121743354291328	40000	5.98	$1.39^{+0.11}_{-0.12}$
Marginal detections of SLF variability:					
[L72] LH 9−89	30275740	4662154018793644928	26700	5.05	$0.80^{+0.37}_{-0.31}$
[ELS2006] N11 051	30275973	4662156630134021376	41400	5.42	$2.50^{+1.11}_{-0.65}$
Sk −66 18	30312045	4662202878335589376	40200	5.55	$2.87^{+1.79}_{-0.82}$
[ELS2006] N11 046	30313090	4662144501145651328	33500	5.21	$1.17^{+1.10}_{-0.43}$
W61 28−5	276936126	4657275137819689216	44000	5.51	$0.93^{+0.18}_{-0.15}$
BI 237	277105480	4660109236409051392	53200	5.83	$1.04^{+6.09}_{-0.29}$
VFTS 244	277300097	4657680552664841856	41050	5.58	$1.87^{+0.48}_{-0.39}$
VFTS 355	277300563	4657688695923883648	43400	5.52	$1.08^{+0.13}_{-0.11}$
Sk −66 100	373849172	4660223379469868416	39000	5.59	$2.75^{+4.79}_{-1.03}$
BI 173	373919576	4658104341338342528	34500	5.60	$2.42^{+4.29}_{-0.95}$

To overcome these challenges, we use the `tglc` software package[4], which allows a user to extract light curves of (faint and blended) TESS targets using an effective point spread function (ePSF) fitting methodology (Han & Brandt 2023). This ePSF method has been shown to be highly effective at disentangling different sources in regions with heavily blended TESS targets because it uses a Bayesian framework with priors for source locations informed by Gaia astrometry (Gaia Collaboration et al. 2016, 2023). We refer the reader to Han & Brandt (2023) for full technical and numerical details of the well-documented and open-source `tglc` software tool. We performed testing against other PSF-fitting software tools (e.g. `photutils`; Bradley et al. 2022), and concluded that the `tglc` software provides, on average, a more robust light curve extraction, especially when compared to standard SAP approaches applied to SMC and LMC massive stars (Van Daele 2023).

As a sanity check, we visually inspected all the diagnostic plots provided by the `tglc` software package and the extracted ePSF light curves for all stars. Unsuccessful cases are easily flagged based on the standard deviation of the extracted ePSF light curve exceeding 50 mmag, which is primarily because such a light curve is dominated by systematics or extremely high Poisson noise levels because it contains very little flux from the stellar target and is dominated by background flux. The typical amplitudes of SLF variability for Galactic massive stars are well below this (e.g. Bowman et al. 2019b, 2020), meaning that unsuccessful cases are easily flagged automatically. In general, we are guided by previous studies of Galactic massive stars with TESS (e.g. Bowman et al. 2020, 2022) in terms of the typical amplitude and period ranges of coherent pulsations and SLF variability in massive stars. Since SMC and LMC massive stars have (much) larger noise levels in their light curves compared to Galactic stars, because they are (much) fainter, we are unable to probe the faintest stars in the XShootU sample, which correspond to the lowest mass stars (i.e. late-B stars). Unfortunately, the majority of the XShootU sample of massive stars are quite faint and/or too heavily blended to extract reliable light curves even with the ePSF methodology.

To be classified as a successful case, a star had to pass all quality checks discussed above, and we also required consistent signatures of variability in its light curve in at least two available TESS sectors. Successful cases were subsequently detrended using a low-order polynomial to remove any remaining long-period instrumental artefacts, which is necessary and typical for TESS mission data (see Bowman et al. 2020, 2022). From the XShootU sample of SMC and LMC stars, we define a sub-sample of 23 successfully-extracted SMC massive stars that are within or proximate to the sub-surface convection zone

[4] `https://github.com/TeHanHunter/TESS_Gaia_Light_Curve`

stability window including asteroseismically calibrated amounts of CBM (cf. Fig. 1). Additionally, we are able to extract reliable light curves for 21 LMC massive stars, but these are all outside of their corresponding sub-surface convection zone stability window. The names and spectroscopic parameters of the sub-samples of SMC and LMC massive stars are provided in Tables 1 and 2, respectively, and the location of these sub-samples in the HR diagram are shown in Fig. 1. We emphasise that the SMC sub-sample includes stars both inside and outside of the sub-surface convection zone stability window, allowing us to investigate differences in the observed SLF variability in the next Section.

4. SLF variability in SMC and LMC massive stars

After having started from the XShootU sample, we have identified a sub-sample of 23 SMC massive stars that satisfy the following criteria: (i) reliable stellar parameters in the literature; (ii) proximate to or within the sub-surface convection zone stability windows that include CBM calibrated by asteroseismology; and (iii) robust ePSF light curves extracted using the `tglc` software package (Han & Brandt 2023). The locations of the SMC and LMC sub-samples in the HR diagram in relation to our calculated evolution tracks and the corresponding sub-surface convection stability window are shown in Fig. 1.

We fit the extracted ePSF light curves using the Gaussian process (GP) regression light curve fitting methodology of Bowman & Dorn-Wallenstein (2022) based on the `celerite2` software package[5] (Foreman-Mackey et al. 2017, 2019). Similar to Bowman & Dorn-Wallenstein (2022) who applied this method to Galactic massive stars, we use a damped simple harmonic oscillator (SHO) kernel with a damping time scale, $\tau_{\rm damp}$, amplitude, σ_A, and characteristic variability time scale, $\rho_{\rm damp}$ (from which a characteristic frequency, $\nu_{\rm char}$, can be calculated), as free parameters, all with large uniform priors. An additional term for the jitter, $C_{\rm w}$ is also included which is related to the amount of white noise in a light curve, which is assigned a Gaussian prior with a width corresponding to standard deviation of the light curve (see Bowman & Dorn-Wallenstein 2022). With best-fit parameters determined by the GP regression method, we then estimate the statistical confidence intervals for all GP regression free parameters using a Hamiltonian Monte-Carlo with a no U-turn sampler (NUTS) using the `pymc3` software package[6] (Salvatier et al. 2016). The resultant $\nu_{\rm char}$ values and their 2σ confidence intervals for the sub-samples of SMC and LMC stars are provided in Tables 1 and 2. This numerical analysis methodology was shown to be more efficient and more robust against systematic uncertainties when analysing SLF variability in Galactic massive stars compared to directly fitting an amplitude spectrum with a Lorentzian-like function (Bowman & Dorn-Wallenstein 2022).

After fitting the light curves for all stars in our SMC and LMC sub-samples, it is immediately clear that all of the stars exhibit SLF variability similar to their Galactic counterparts (e.g. Bowman et al. 2019a,b, 2020). Therefore, we demonstrate for the first time that SLF variability is also seemingly ubiquitous across a wide range in metallicity, as well as mass and age. We show the TESS light curves, frequency spectra and corresponding GP regression model for the SMC and LMC sub-samples of stars in Figs. A.1–A.3 and A.4–A.6, respectively. For comparison, we define a third sub-sample of Galactic massive stars based on the best-fitting GP regression models for 30 massive stars in the Milky Way from Bowman & Dorn-Wallenstein (2022). We find similar morphologies of SLF variability for all stars in all three sub-samples, SMC, LMC and Galactic, regardless of whether they are located inside or outside of their corresponding stability windows. However some of stars in both the SMC and LMC sub-samples have only marginal detections of SLF variability owing to relatively high levels of Poisson (i.e. white) noise in their light curves. But these are the faintest stars and are typically beyond the nominal operating brightness limit of TESS around $V \gtrsim 13$ mag. Hence it is not reasonable to draw inference from stars fainter than these since their light curves are dominated by white noise and instrumental systematics.

We show histograms of the important GP regression fitting parameters for all the massive stars across the Milky Way, LMC and SMC sub-samples in Fig. 2. Interestingly, the amplitude of the SLF variability is slightly lower on average for the SMC sub-sample of massive stars compared to the LMC. This is achieved by defining a signal-to-noise ratio (SNR) of SLF variability as the ratio of the maximum and minimum values in the PSD of the GP regression fit. This serves as a useful proxy for $\alpha_0/C_{\rm W}$ (cf. Bowman et al. 2020) and allows a comparison of stars with very different white noise contributions in their light curves. For example, the inferred value of the amplitude of the SLF variability in a frequency spectrum (i.e. α_0) in SMC stars can be artificially higher if inferred from directly fitting a frequency spectrum because of the increased contribution of white noise (i.e. $C_{\rm W}$), which can be large within the sub-sample of SMC stars. With the caveat of it being a small sample of stars to compare, the histograms in Fig. 2 show similar values for SNR, characteristic frequency, $\nu_{\rm char}$, damping timescale, $\tau_{\rm damp}$, or quality factor, Q, across the three metallicity regimes.

To further demonstrate the common morphology of SLF variability across all metallicity regimes, the correlations among the SNR, characteristic frequency, $\nu_{\rm char}$, and damping timescale, $\tau_{\rm damp}$, of the SLF variability for the sub-samples of Galactic, LMC and SMC massive stars studied in this work are colour-coded by luminosity and shown in Fig. 3. For the Milky Way sub-sample stars, we use the spectroscopic effective luminosity with values from Bowman et al. (2020), which is defined as $\mathscr{L} := T_{\rm eff}^4/g$ (Langer & Kudritzki 2014), due to uncertain values in galactic extinction and reddening and to be consistent with the previous analyses of SLF variability across the HR diagram in this series of papers. Indeed, the photometric and GP regression fitting parameters are less precise for the LMC and SMC sub-samples owing to the noisier TESS light curves, but the same trends in Fig. 3 exist in all three sub-samples. As noted by previous studies, the diversity in SLF variability parameters is high, and could be linked to different rotation rates or inclinations of the stars, which give rise to different surface amplitudes of IGWs (see Bowman & Dorn-Wallenstein 2022). Yet the similar correlations across all metallicity regimes support a common physical origin for SLF variability that is largely insensitive to metallicity. Moreover, massive low-metallicity stars that are luminous have, on average, lower $\nu_{\rm char}$ values as previously demonstrated for Galactic massive stars (Bowman et al. 2019b, 2020).

These results lead to two possible conclusions. First, the similar morphology for stars inside and outside of their respective sub-surface convection stability windows across all three metallicity regimes indicates that SLF variability is unlikely to be exclusively caused by sub-surface convection, assuming that the stability windows (cf. Section 2) are based on an accurate implementation of physics in 1D structure models, and thus can act as good predictors of observables. Second, if SLF variabil-

[5] `https://celerite2.readthedocs.io/en/latest/`
[6] `https://docs.pymc.io/en/v3/index.html`

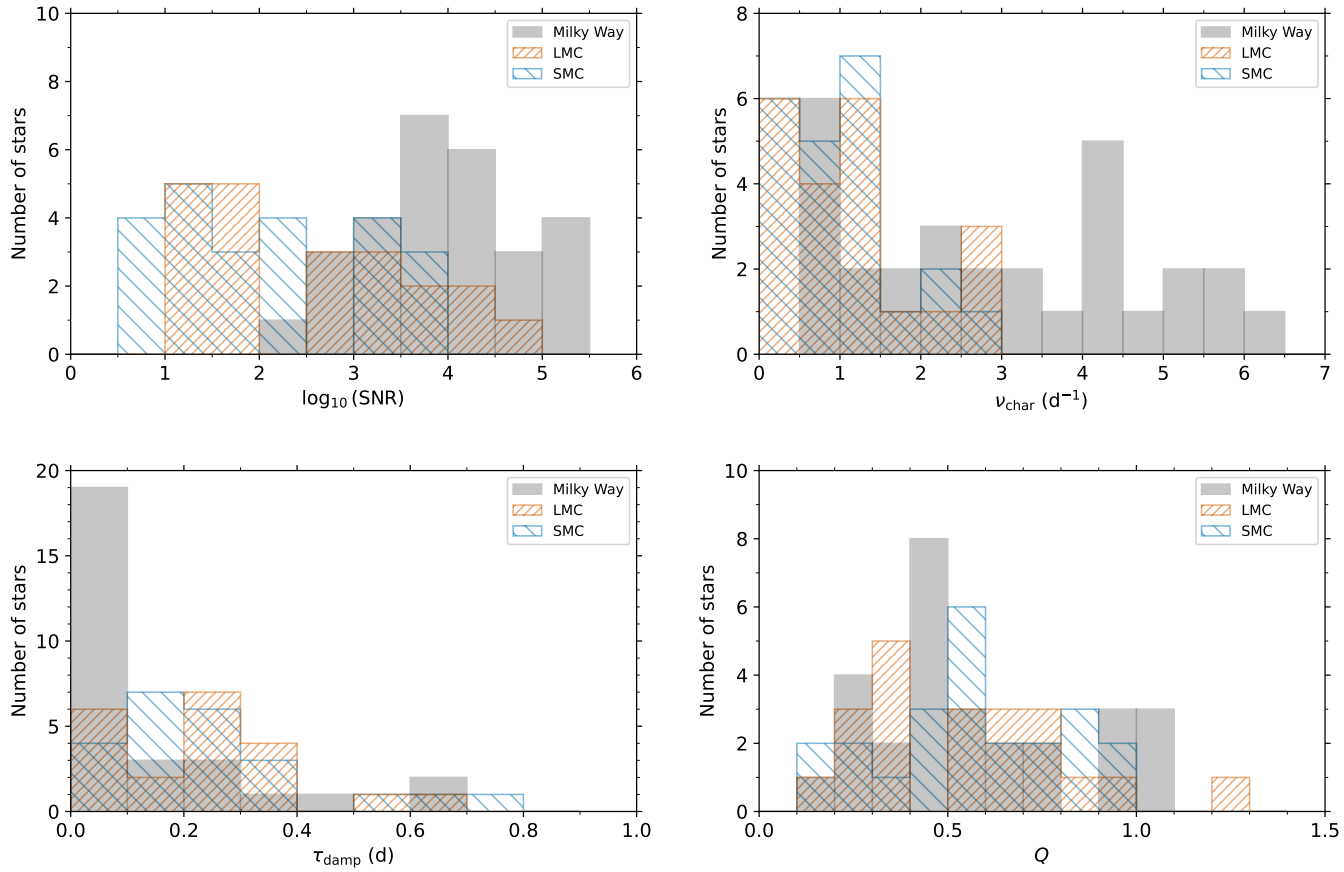

Fig. 2. Histograms of the signal-to-noise ratio (SNR), characteristic frequency, $\nu_{\rm char}$, damping timescale, $\tau_{\rm damp}$, and the quality factor, Q, of SLF variability for the Milky Way, LMC and SMC massive stars.

ity is in fact caused by sub-surface convection, these results imply that non-rotating 1D structure models do not provide reasonable predictors for observables associated with SLF variability. Of course, both of these conclusions may be correct, which emphasises the need to continue to compare observations to hydrodynamical simulations of stellar interiors with 3D spherical geometry and realistic rotation rates (e.g. Aerts & Rogers 2015; Bowman et al. 2019a,b; Edelmann et al. 2019; Vanon et al. 2023; Anders et al. 2023; Thompson et al. 2024).

On the other hand, since the SNR of SLF variability is somewhat lower for SMC stars compared to LMC and Galactic massive stars, it is a reasonable inference that the observed SLF variability arises from both core convection and sub-surface convection. For LMC and Galactic stars, and their marginally larger SLF variability amplitudes and their more efficient sub-surface convection zones, the observed SLF variability could be comprised of IGWs from both core convection and sub-surface convection. Whereas, for SMC stars with their marginally smaller SLF variability amplitudes and their less efficient sub-surface convection zones, the observed SLF variability could be exclusively caused by IGWs from core convection. Therefore, on balance, these results support the conclusion that 1D structure models cannot be used to rule out core convection as a contributing factor to SLF variability, even if it is arguably not the dominant contributor for Galactic massive stars, which remains to be seen. In addition to metallicity, it is expected from stellar evolution theory and models that sub-surface convection is more important for stars approaching the TAMS given the evolutionary changes to their structures are more conducive to this mechanism than compared to stars near the ZAMS (Bowman 2023).

5. Discussion and Conclusions

In this work, we have demonstrated for the first time that SLF variability is omnipresent in massive stars in low-metallicity environments when sufficiently high-quality light curves are available. We achieved this using a sub-sample of massive stars in the SMC and LMC galaxies, which were included as targets within the ongoing XShootU collaboration (Vink et al. 2023). We have extracted optimised ePSF light curves from the TESS mission FFI data using the `tglc` software package (Han & Brandt 2023), and fit them using a GP regression fitting methodology (Bowman & Dorn-Wallenstein 2022). We find that all SMC massive stars have similar SLF variability morphologies to each other, but also to LMC and Galactic massive stars (Bowman et al. 2019b, 2020; Bowman & Dorn-Wallenstein 2022). Hence, this demonstrates that the physical mechanism(s) responsible for SLF variability in massive stars appears to be largely independent of a star's metallicity, and predominantly set by a star's location in the HR diagram (i.e. a star's mass and radius).

We also find that the morphology of SLF variability in massive stars does not depend on whether a star is within the stability window for sub-surface convection predicted by non-rotating 1D structure models. These stability windows are defined based on the Rayleigh number for convection (Jermyn et al. 2022), and have been updated in this work to include asteroseismically

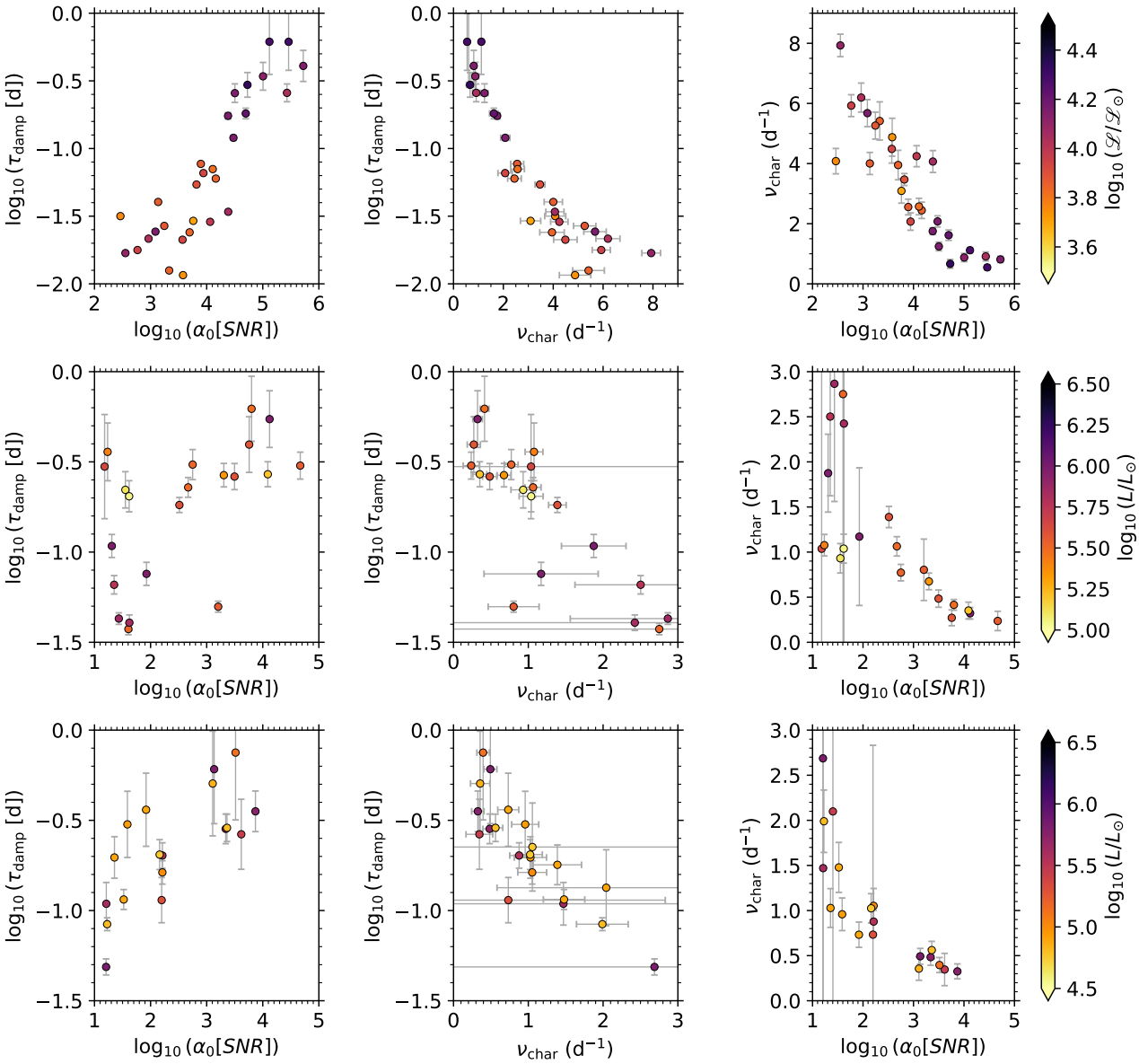

Fig. 3. Correlations between (spectroscopic) luminosity and SLF variability parameters for the sub-samples of Milky Way, LMC and SMC massive stars studied in this work are shown in panels from top to bottom, respectively. Note that spectroscopic effective luminosity is defined as $\mathscr{L} := T_{\rm eff}^4/g$ (Langer & Kudritzki 2014) with values taken from Bowman et al. (2020) for consistency purposes. Uncertainties plotted are the 2σ confidence intervals from the combined methodology of a GP regression and Hamiltonian Monte-Carlo with a no U-turn sampler (Bowman & Dorn-Wallenstein 2022).

calibrated constraints on interior mixing (Bowman 2020). We emphasise that the approach by Jermyn et al. (2022) to use the Rayleigh number as a definition for the onset of convection produces larger stability windows for SMC and LMC stars compared to Milky Way stars because of their lower metallicities. Of course, owing to the small size of the LMC stability window, it is clear that none of the stars studied in this work fall inside the corresponding sub-surface convection zone stability window even if relatively large confidence intervals for their spectroscopic estimates of effective temperature and luminosity are considered. On the other hand, the fact that the SMC sub-sample includes stars both inside and outside of the corresponding sub-surface convection zone stability window and have similar SLF variability is a challenge to using non-rotating 1D structure models for predictions of sub-surface convection as a universal explanation for SLF variability.

Important limitations of the 1D structure models used in this work and elsewhere in the literature include the lack of rotation, but also uncertainties in opacity tables for stellar interiors (see discussion by Aerts et al. 2018), which may lead to smaller or larger stability windows dependent on how the physical prescriptions for these processes are incorporated in 1D structure models. This has not been investigated and is the subject of future work. For example, rotation breaks the assumption of spherical symmetry and leads to gravity darkening, which would arguably lead to different depths for sub-surface convection as a function of stellar latitude. By extension, this could lead to different SLF variability amplitudes as a function of latitude, meaning one could expect different properties for SLF variability for stars of different inclinations with respect to the observer. Moreover, 1D stellar structure models, including those calculated in this work use mixing-length theory, which has limitations in mod-

elling the true dynamics of convective zones — see review by Joyce & Tayar (2023).

A complementary result of this work is that we do not find any convincing cases of massive stars with coherent pulsation modes excited by the heat-engine mechanism in the LMC and SMC targets considered. Studies that combine time-series spectroscopy (i.e. identify spectral line profile variability) with photometry have yielded a lower incidence rate of β Cep and SPB pulsators and a higher incidence rate of pulsating Be stars in the SMC compared to the galaxy (see e.g. Diago et al. 2008). The lower opacities of SMC and LMC massive stars is a natural explanation for a less efficient heat-engine mechanism exciting coherent pulsation modes (e.g. Salmon et al. 2012). However, predictions of pulsation excitation mechanism based on 1D stellar structure models typically lack rotation and atomic diffusion including radiative levitation, which have both been shown to be important in exciting coherent pulsation modes in Galactic main-sequence B-type stars (Townsend 2005; Szewczuk & Daszyńska-Daszkiewicz 2017; Rehm et al. 2024). Interestingly, the reduced incidence of coherent pulsators in the literature and lack of coherent pulsators in our sample further supports the conclusion of weaker sub-surface convection zones for low-metallicity stars. Therefore, a natural next step on the theoretical side is to include rotation and atomic diffusion including radiative levitation in the calculations of sub-surface convection zone stability windows for low-metallicity massive stars.

The physical mechanism behind SLF variability in massive stars is debated in the literature, but all currently proposed mechanisms have advantages and limitations when confronted with observations — see review by Bowman (2023). A much larger sample of SMC massive stars with accurate stellar parameters is expected in the near future and will be highly advantageous to further explore the physical mechanisms responsible for SLF variability, which is incorporated within the XShootU (Vink et al. 2023) and BLoEM (Shenar et al. 2024) projects. Regardless, our proof-of-concept study demonstrates it is possible to probe the excitation mechanism of SLF variability at low metallicity and constrain its dependence on a star's location in the HR diagram. Equally, our results also demonstrate the limitations of using non-rotating 1D structure models for producing observables to be compared to observations of SLF variability.

Finally, our study provides strong motivation for hydrodynamicists to perform low-metallicity simulations of massive stars in 3D spherical geometry and including realistic rotation rates, since this may elucidate the latitudinal properties of IGWs excited by sub-surface convection and core convection. We postulate that the high diversity in SLF variability morphologies is caused by a combination of unknown inclination angles combined with a large range in rotational velocities. Thus a range of latitudinally dependent interior mixing efficiencies may be at work, which are not well calibrated in massive star evolution theory. Specifically addressing how convective zones produce SLF variability in 3D spherical geometry including rotation is required in order to accurately compare predicted amplitudes and frequencies of IGWs to observations. In this study, the omnipresence of SLF variability across a large range in metallicity suggests that sub-surface convection may play a minor role, especially for younger and lower metallicity massive stars. In the future, a much larger sample of massive stars in the SMC and LMC with accurate spectroscopic parameters delivered by the XShootU and BLoEM projects combined with hydrodynamical simulations will allow a new and exciting dimension to be added to the growing interest in massive star variability studies.

Acknowledgements. The authors thank Adam Jermyn for useful discussions and kindly providing well-documented and open-access MESA inlists, as well as Daniel Lecoanet and Matteo Cantiello for useful discussions during the 'Probes of Transport in Stars' workshop hosted at KITP in 2021. This research was supported in part by the National Science Foundation (NSF) under Grant Number NSF PHY-1748958. DMB gratefully acknowledges funding from the Research Foundation Flanders (FWO) by means of a senior postdoctoral fellowship (grant agreement No. 1286521N), an FWO long stay travel grant (agreement No. V411621N), as well as UK Research and Innovation (UKRI) in the form of a Frontier Research grant under the UK government's ERC Horizon Europe funding guarantee (SYMPHONY; grant number: EP/Y031059/1), and a Royal Society University Research Fellowship (URF; grant number: URF\R1\231631). MM gratefully acknowledges funding from FWO by means of a PhD scholarship (11F7120N), and TVR gratefully acknowledges the KU Leuven Research Council (C16/18/005: PARADISE). The authors thank the TESS science team for the excellent data, which were obtained from the Mikulski Archive for Space Telescopes (MAST) at the Space Telescope Science Institute (STScI), which is operated by the Association of Universities for Research in Astronomy, Inc., under NASA contract NAS5-26555. Support to MAST for these data is provided by the NASA Office of Space Science via grant NAG5-7584 and by other grants and contracts. Funding for the TESS mission is provided by the NASA Explorer Program. This research has made use of the SIMBAD database, operated at CDS, Strasbourg, France; the SAO/NASA Astrophysics Data System; and the VizieR catalog access tool, CDS, Strasbourg, France. This research has made use of the following software packages: `matplotlib` (Hunter 2007), `seaborn` (Waskom 2021), `numpy` (Oliphant 2006; van der Walt et al. 2011; Harris et al. 2020), `tglc` (Han & Brandt 2023), `celerite2` (Foreman-Mackey et al. 2017), and `pymc3` (Salvatier et al. 2016).

References

Aerts, C. 2021, Reviews of Modern Physics, 93, 015001
Aerts, C., Christensen-Dalsgaard, J., & Kurtz, D. W. 2010, Asteroseismology (Springer)
Aerts, C., Molenberghs, G., Michielsen, M., et al. 2018, ApJS, 237, 15
Aerts, C. & Rogers, T. M. 2015, ApJ, 806, L33
Aerts, C., Thoul, A., Daszyńska, J., et al. 2003, Science, 300, 1926
Anders, E. H., Lecoanet, D., Cantiello, M., et al. 2023, Nature Astronomy, 7, 1228
Auvergne, M., Bodin, P., Boisnard, L., et al. 2009, A&A, 506, 411
Blomme, R., Mahy, L., Catala, C., et al. 2011, A&A, 533, A4
Borucki, W. J., Koch, D., Basri, G., et al. 2010, Science, 327, 977
Bouret, J. C., Lanz, T., Martins, F., et al. 2013, A&A, 555, A1
Bowman, D. M. 2020, Frontiers in Astronomy and Space Sciences, 7, 70
Bowman, D. M. 2023, Ap&SS, 368, 107
Bowman, D. M., Aerts, C., Johnston, C., et al. 2019a, A&A, 621, A135
Bowman, D. M., Burssens, S., Pedersen, M. G., et al. 2019b, Nature Astronomy, 3, 760
Bowman, D. M., Burssens, S., Simón-Díaz, S., et al. 2020, A&A, 640, A36
Bowman, D. M. & Dorn-Wallenstein, T. Z. 2022, A&A, 668, A134
Bowman, D. M., Vandenbussche, B., Sana, H., et al. 2022, A&A, 658, A96
Bradley, L., Sipőcz, B., Robitaille, T., et al. 2022, astropy/photutils: 1.5.0
Briquet, M., Aerts, C., Baglin, A., et al. 2011, A&A, 527, A112
Briquet, M., Neiner, C., Aerts, C., et al. 2012, MNRAS, 427, 483
Burssens, S., Bowman, D. M., Michielsen, M., et al. 2023, Nature Astronomy, 7, 913
Burssens, S., Simón-Díaz, S., Bowman, D. M., et al. 2020, A&A, 639, A81
Cantiello, M., Langer, N., Brott, I., et al. 2009, A&A, 499, 279
Cantiello, M., Lecoanet, D., Jermyn, A. S., & Grassitelli, L. 2021, ApJ, 915, 112
Degroote, P., Aerts, C., Ollivier, M., et al. 2009, A&A, 506, 471
Diago, P. D., Gutiérrez-Soto, J., Fabregat, J., & Martayan, C. 2008, A&A, 480, 179
Dupret, M.-A., Thoul, A., Scuflaire, R., et al. 2004, A&A, 415, 251
Dziembowski, W. A., Moskalik, P., & Pamyatnykh, A. A. 1993, MNRAS, 265, 588
Dziembowski, W. A. & Pamyatnykh, A. A. 1993, MNRAS, 262, 204
Dziembowski, W. A. & Pamyatnykh, A. A. 2008, MNRAS, 385, 2061
Edelmann, P. V. F., Ratnasingam, R. P., Pedersen, M. G., et al. 2019, ApJ, 876, 4
Foreman-Mackey, D., Agol, E., Ambikasaran, S., & Angus, R. 2017, AJ, 154, 220
Foreman-Mackey, D., Agol, E., Angus, R., et al. 2019, dfm/celerite: celerite v0.3.1
Gaia Collaboration, Prusti, T., de Bruijne, J. H. J., et al. 2016, A&A, 595, A1
Gaia Collaboration, Vallenari, A., Brown, A. G. A., et al. 2023, A&A, 674, A1
Han, T. & Brandt, T. D. 2023, AJ, 165, 71
Harris, C. R., Millman, K. J., van der Walt, S. J., et al. 2020, Nature, 585, 357
Hawcroft, C., Sana, H., Mahy, L., et al. 2023, arXiv e-prints, arXiv:2303.12165

Herwig, F., Woodward, P. R., Mao, H., et al. 2023, MNRAS, 525, 1601
Horst, L., Edelmann, P. V. F., Andrássy, R., et al. 2020, A&A, 641, A18
Howell, S. B., Sobeck, C., Haas, M., et al. 2014, PASP, 126, 398
Hunter, I., Brott, I., Lennon, D. J., et al. 2008, ApJ, 676, L29
Hunter, J. D. 2007, Computing in Science and Engineering, 9, 90
Jenkins, J. M., Twicken, J. D., McCauliff, S., et al. 2016, in Proc. SPIE, Vol. 9913, Software and Cyberinfrastructure for Astronomy IV, 99133E
Jermyn, A. S., Anders, E. H., & Cantiello, M. 2022, ApJ, 926, 221
Jermyn, A. S., Bauer, E. B., Schwab, J., et al. 2023, ApJS, 265, 15
Joyce, M. & Tayar, J. 2023, Galaxies, 11, 75
Koch, D. G., Borucki, W. J., Basri, G., et al. 2010, ApJ, 713, L79
Krtička, J. & Feldmeier, A. 2018, A&A, 617, A121
Krtička, J. & Feldmeier, A. 2021, A&A, 648, A79
Langer, N. & Kudritzki, R. P. 2014, A&A, 564, A52
Le Saux, A., Baraffe, I., Guillet, T., et al. 2023, MNRAS, 522, 2835
Lecoanet, D., Bowman, D. M., & Van Reeth, T. 2022, MNRAS, 512, L16
Lecoanet, D., Cantiello, M., Anders, E. H., et al. 2021, MNRAS, 508, 132
Lecoanet, D., Cantiello, M., Quataert, E., et al. 2019, ApJ, 886, L15
Michielsen, M., Aerts, C., & Bowman, D. M. 2021, A&A, 650, A175
Miglio, A., Montalbán, J., & Dupret, M.-A. 2007, MNRAS, 375, L21
Mokiem, M. R., de Koter, A., Evans, C. J., et al. 2007, A&A, 465, 1003
Mokiem, M. R., de Koter, A., Evans, C. J., et al. 2006, A&A, 456, 1131
Oliphant, T. E. 2006, A guide to NumPy, Vol. 1 (Trelgol Publishing USA)
Pamyatnykh, A. A., Handler, G., & Dziembowski, W. A. 2004, MNRAS, 350, 1022
Paxton, B., Bildsten, L., Dotter, A., et al. 2011, ApJS, 192, 3
Paxton, B., Cantiello, M., Arras, P., et al. 2013, ApJS, 208, 4
Paxton, B., Marchant, P., Schwab, J., et al. 2015, ApJS, 220, 15
Paxton, B., Schwab, J., Bauer, E. B., et al. 2018, ApJS, 234, 34
Paxton, B., Smolec, R., Schwab, J., et al. 2019, ApJS, 243, 10
Pedersen, M. G., Aerts, C., Pápics, P. I., et al. 2021, Nature Astronomy, 5, 715
Ramírez-Agudelo, O. H., Simón-Díaz, S., Sana, H., et al. 2013, A&A, 560, A29
Ratnasingam, R. P., Edelmann, P. V. F., & Rogers, T. M. 2019, MNRAS, 482, 5500
Ratnasingam, R. P., Edelmann, P. V. F., & Rogers, T. M. 2020, MNRAS, 497, 4231
Ratnasingam, R. P., Rogers, T. M., Chowdhury, S., et al. 2023, A&A, 674, A134
Rehm, R., Mombarg, J. S. G., Aerts, C., et al. 2024, arXiv e-prints, arXiv:2405.08864
Ricker, G. R., Winn, J. N., Vanderspek, R., et al. 2015, Journal of Astronomical Telescopes, Instruments, and Systems, 1, 014003
Rogers, T. M. 2015, ApJ, 815, L30
Rogers, T. M., Lin, D. N. C., McElwaine, J. N., & Lau, H. H. B. 2013, ApJ, 772, 21
Roman-Duval, J., Proffitt, C. R., Taylor, J. M., et al. 2020, Research Notes of the American Astronomical Society, 4, 205
Salmon, S., Montalbán, J., Morel, T., et al. 2012, MNRAS, 422, 3460
Salmon, S. J. A. J., Moyano, F. D., Eggenberger, P., Haemmerlé, L., & Buldgen, G. 2022, A&A, 664, L1
Salvatier, J., Wieckiâ, T. V., & Fonnesbeck, C. 2016, PyMC3: Python probabilistic programming framework
Sana, H., de Mink, S. E., de Koter, A., et al. 2012, Science, 337, 444
Schultz, W. C., Bildsten, L., & Jiang, Y.-F. 2022, ApJ, 924, L11
Shenar, T., Bodensteiner, J., Sana, H., et al. 2024, in prep
Szewczuk, W. & Daszyńska-Daszkiewicz, J. 2017, MNRAS, 469, 13
Thompson, W., Herwig, F., Woodward, P. R., et al. 2024, MNRAS, 531, 1316
Townsend, R. H. D. 2005, MNRAS, 364, 573
Van Daele, P. 2023, Master's thesis, KU Leuven, Belgium
van der Walt, S., Colbert, S. C., & Varoquaux, G. 2011, Computing in Science Engineering, 13, 22
Vanlaer, V., Das, S. B., Bugnet, L., et al. 2024, A&A, in prep
Vanon, R., Edelmann, P. V. F., Ratnasingam, R. P., Varghese, A., & Rogers, T. M. 2023, ApJ, 954, 171
Varghese, A., Ratnasingam, R. P., Vanon, R., Edelmann, P. V. F., & Rogers, T. M. 2023, ApJ, 942, 53
Vernet, J., Dekker, H., D'Odorico, S., et al. 2011, A&A, 536, A105
Vink, J. S., Mehner, A., Crowther, P. A., et al. 2023, A&A, 675, A154
Waskom, M. L. 2021, Journal of Open Source Software, 6, 3021
Weiss, W. W., Rucinski, S. M., Moffat, A. F. J., et al. 2014, PASP, 126, 573
Weiss, W. W., Zwintz, K., Kuschnig, R., et al. 2021, Universe, 7, 199
Zwintz, K., Pigulski, A., Kuschnig, R., et al. 2024, A&A, 683, A49

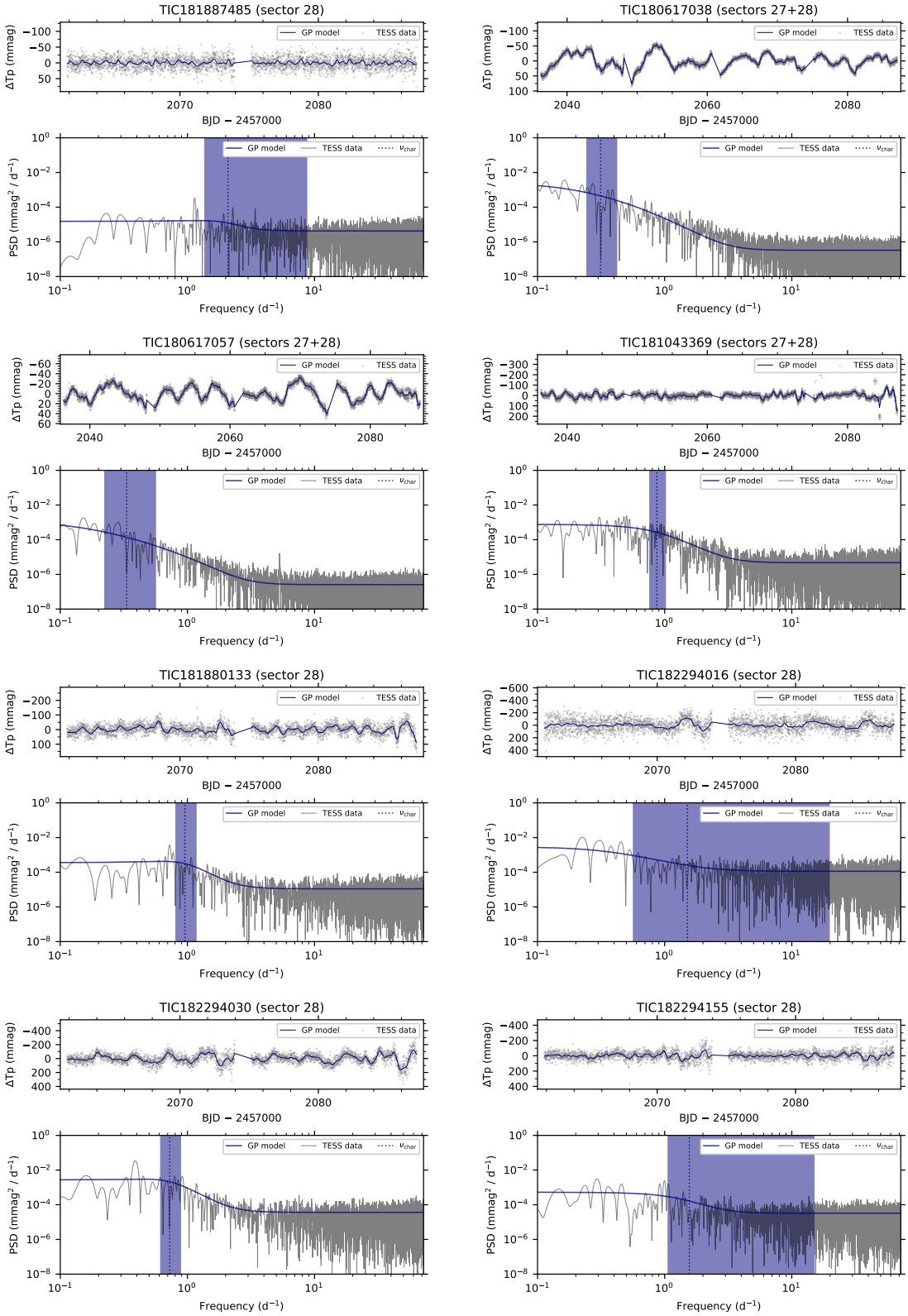

Fig. A.1. Extracted ePSF light curves using `tglc` (Han & Brandt 2023) and fitted with the GP regression methodology of Bowman & Dorn-Wallenstein (2022) for SMC massive stars.

Appendix A: Figures

The extracted ePSF light curves using the `tglc` software package (Han & Brandt 2023) fitted with the GP regression methodology of Bowman & Dorn-Wallenstein (2022) for SMC and LMC massive stars are shown in Figs. A.1–A.3 and Figs. A.4–A.6, respectively.

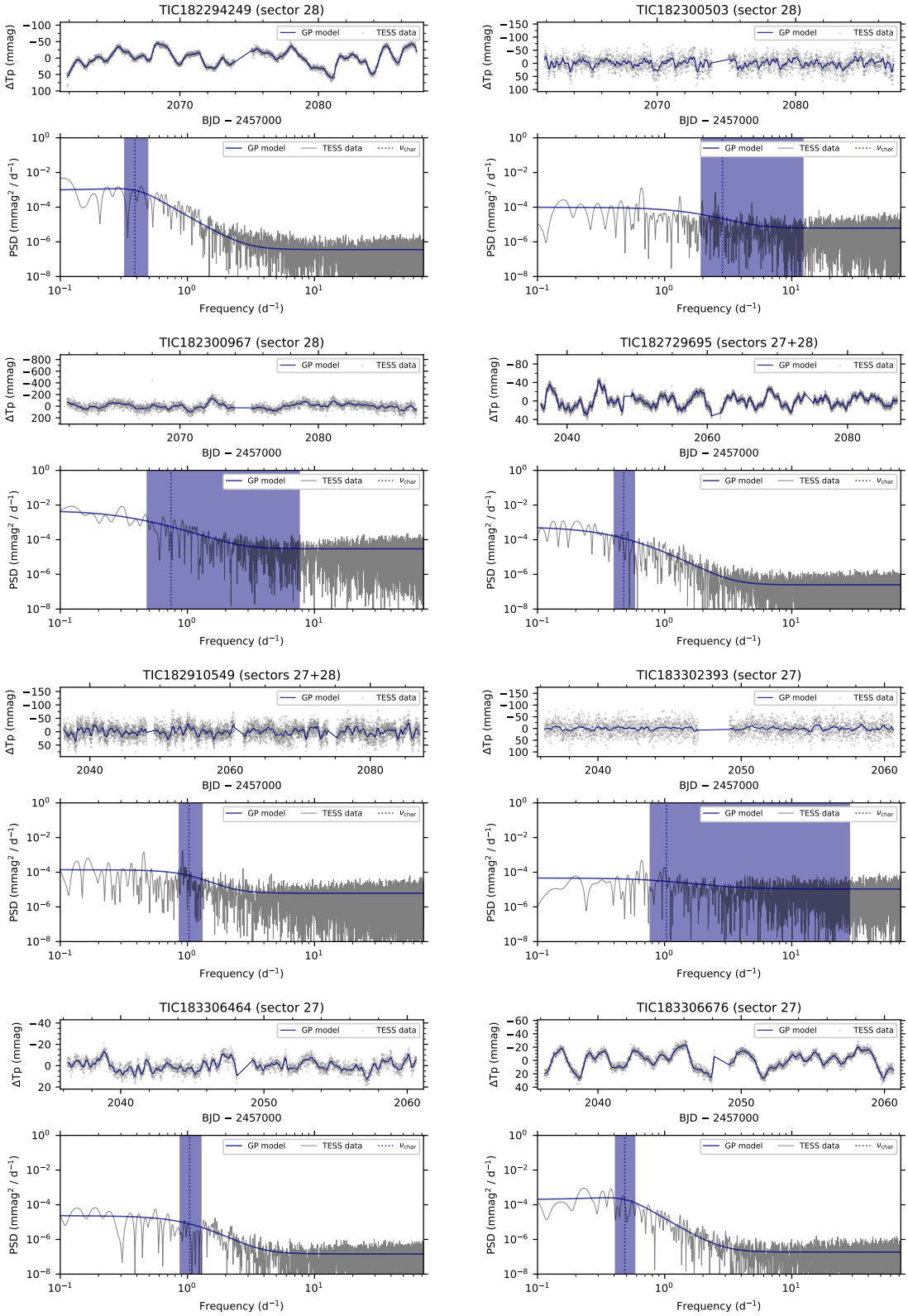

Fig. A.2. Extracted ePSF light curves using `tglc` (Han & Brandt 2023) and fitted with the GP regression methodology of Bowman & Dorn-Wallenstein (2022) for SMC massive stars *(continued)*.

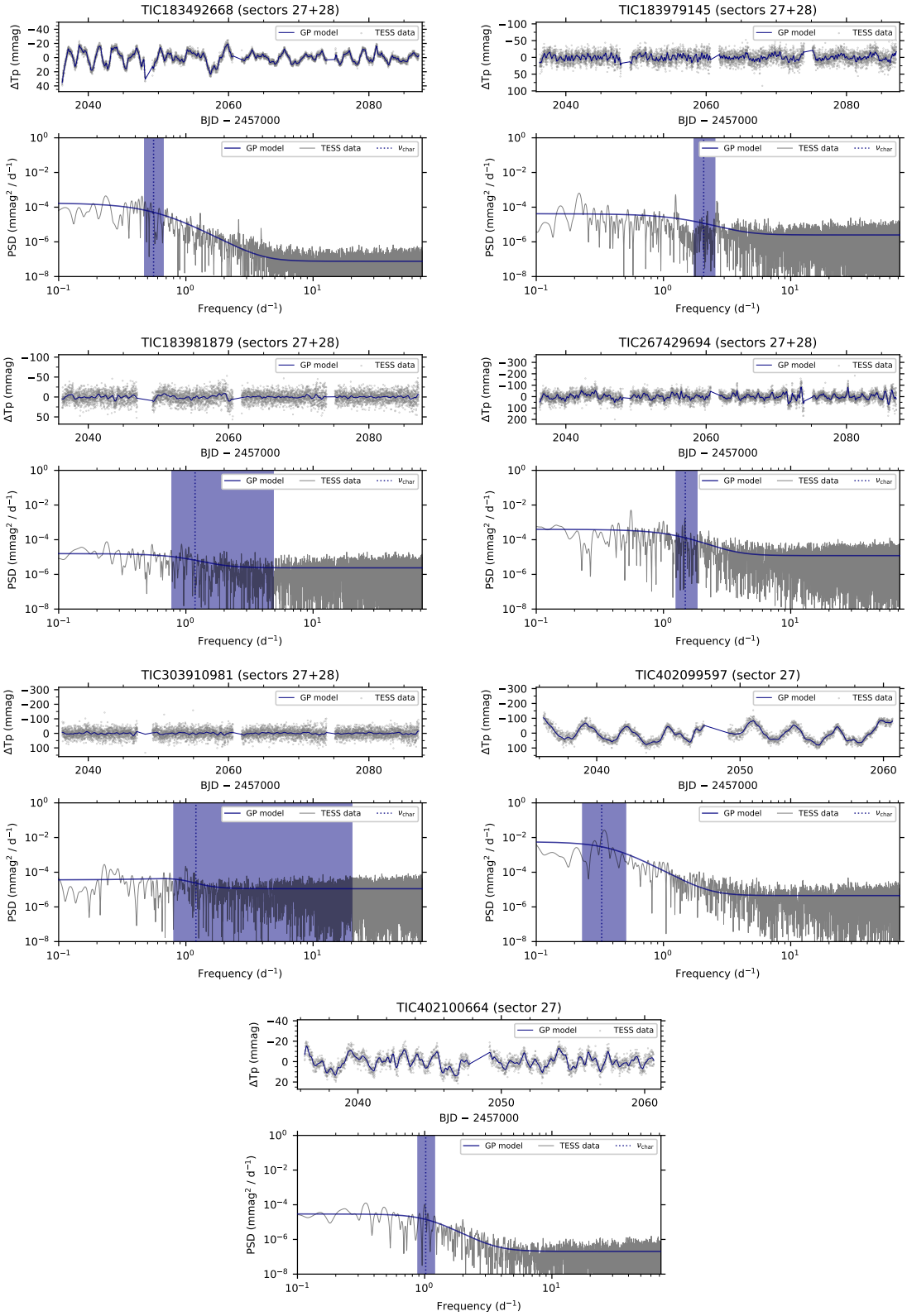

Fig. A.3. Extracted ePSF light curves using `tglc` (Han & Brandt 2023) and fitted with the GP regression methodology of Bowman & Dorn-Wallenstein (2022) for SMC massive stars *(continued)*.

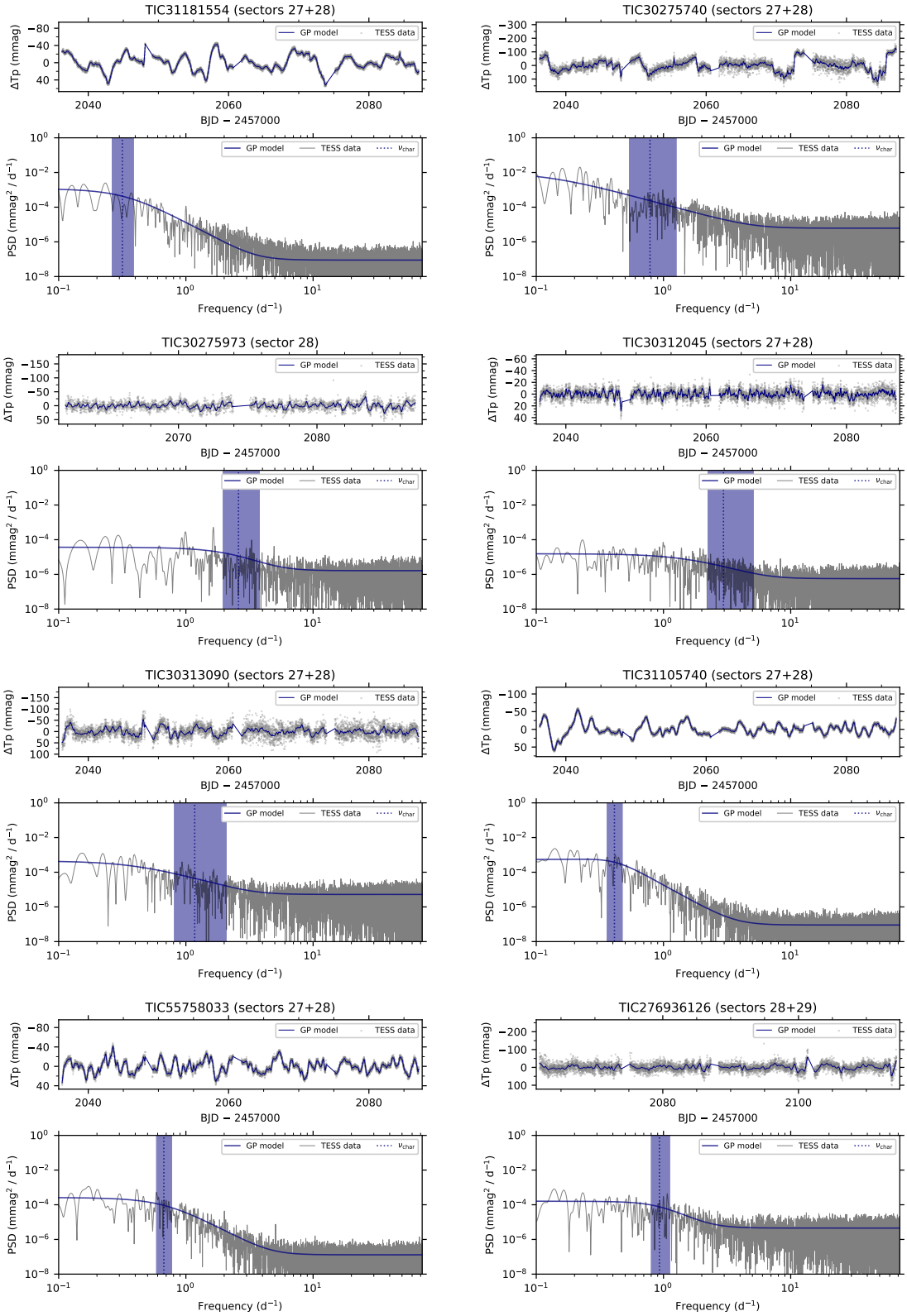

Fig. A.4. Extracted ePSF light curves using `tglc` (Han & Brandt 2023) and fitted with the GP regression methodology of Bowman & Dorn-Wallenstein (2022) for LMC massive stars.

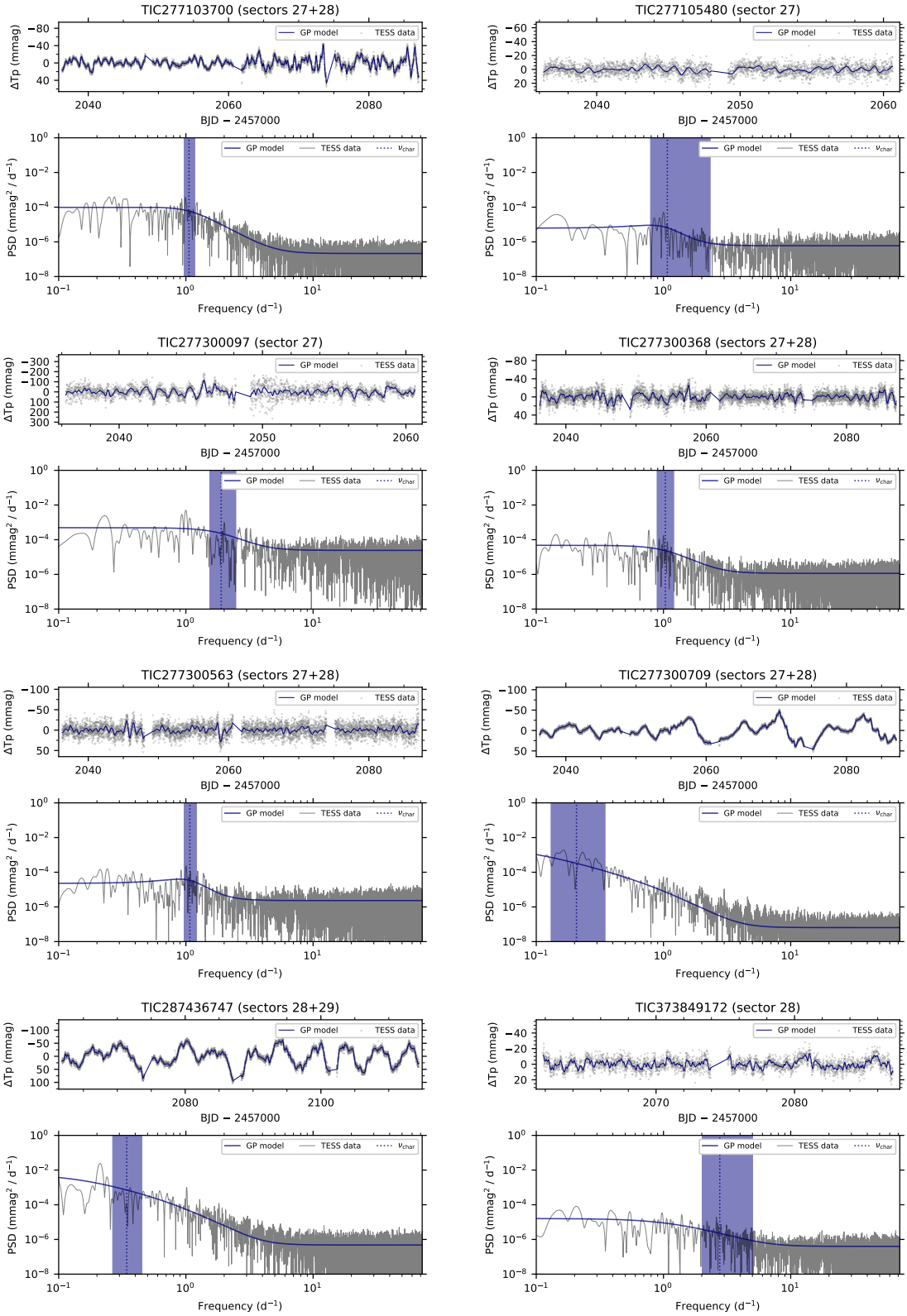

Fig. A.5. Extracted ePSF light curves using `tglc` (Han & Brandt 2023) and fitted with the GP regression methodology of Bowman & Dorn-Wallenstein (2022) for LMC massive stars *(continued)*.

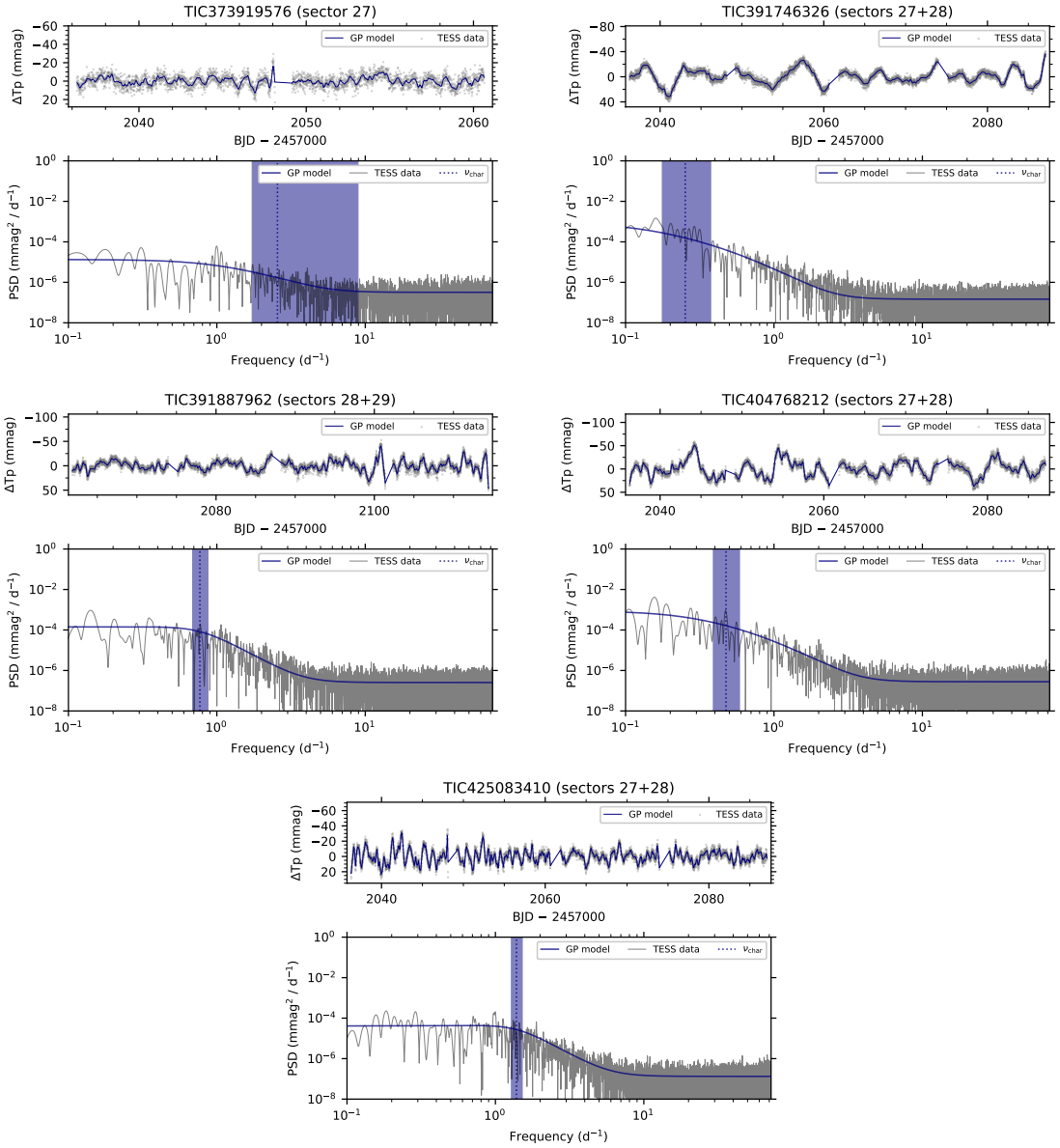

Fig. A.6. Extracted ePSF light curves using `tglc` (Han & Brandt 2023) and fitted with the GP regression methodology of Bowman & Dorn-Wallenstein (2022) for LMC massive stars *(continued)*.